J|A|C|S
ARTICLES
Published on Web 04/09/2003

Adsorption Morphology, Light Absorption, and Sensitization Yields for Squaraine Dyes on SnS_2 Surfaces

Norihiko Takeda† and Bruce A. Parkinson*

Contribution from the Department of Chemistry, Colorado State University, Fort Collins, Colorado 80523-1872

Received July 24, 2002; E-mail: bruce.parkinson@colostate.edu

Abstract: The sensitization properties of two squaraine dyes adsorbed onto the van der Waals surface of *n*-doped tin disulfide single crystals were studied using atomic force microscopy (AFM), vis−NIR absorption spectroscopy, and photoelectrochemical techniques. Quantum yield per absorbed photon (QYAP) values of near unity were observed for submonolayer coverages of 2,4-bis(4-(*N*-methyl-*N*-hexylamino)phenyl)-squaraine (1-6SQ) in aqueous electrolyte when a sufficiently positive bias was applied, demonstrating the advantages of SnS_2 as a photoanode for fundamental studies of dye sensitization. Islandlike and microcrystalline morphologies, associated with aggregate formation and revealed by AFM, could be correlated with spectral shifts in both the absorbance and photoaction spectra. A related dye, 2,4-bis(4-(*N*,*N*-dimethyl)-2-hydroxyphenyl)squaraine (1-1OHSQ), at similar coverages showed slightly lower QYAP, ascribed to a recombination path due to the different aggregate structures.

Introduction

Dye sensitization of large band gap semiconductors has been extensively studied from both a fundamental perspective, investigating interfacial electron-transfer processes, and its practical importance.[1−4] Electron injection from excited states of dyes into the conduction band of semiconductors is one of the principal processes of silver-halide-based photography[5] and is also a key element of possible solar-to-electrical energy conversion devices.[6−8] In the latter case, photooxidized dyes are regenerated by a redox species in the contacting solution to ensure continuous operation of these devices. High incident photons-to-current conversion efficiencies (IPCE > 75%) were observed for thin films of high surface area nanocrystalline TiO_2 onto which a Ru-based inorganic dye was adsorbed. These "Grätzel cells" have also shown high solar-to-electrical power conversion efficiencies and stabilities in sunlight.[6−8] Sensitized photocurrent quantum yield per absorbed photon (QYAP) values approaching 100% were deduced for organic dyes adsorbed onto van der Waals surfaces of single crystals of WSe_2 and SnS_2 from solutions containing the dyes.[9,10] Very fast electron injection rates from the adsorbed dyes into the semiconductor conduction band are essential for realizing the high quantum yields, since the recombination of electron−hole pairs competes with photocurrent generation. In previous investigations, the formation of dye monolayers was assumed based on Langmuir-like adsorption but the actual dye coverages or morphologies were not directly measured.[9,10]

Dyes adsorbed on semiconductor surfaces could be monomeric, aggregated, or a mixture of these forms and, in addition, could have different orientations of their chromophores with respect to the substrate (i.e., flat or edge on). Dye aggregates show different photophysical and photochemical properties depending on their molecular order and aggregate sizes.[11−14] For example, J-aggregates of cyanine dyes on silver halide microcrystals are important for color photography due to their intense, sharp, and red-shifted absorption bands when compared to those of the dye monomers. J-aggregrates have a high sensitivity and wavelength selectivity for the exposing light. Some cyanine dyes form H-aggregates, with a blue-shifted absorption spectrum. The spectral shifts are attributed to the strong coupling of the transition dipoles via excitonic interaction between the ordered dye molecules. Formation of H- and J-aggregates of cyanine dyes has been deduced mainly from their electronic absorption spectra and from molecular exciton theory.[14,15]

† Present address: Brookhaven National Laboratory, Chemistry Department, Upton, NY 11973-5000.

(1) Gerischer, H.; Willig, F. *Top. Curr. Chem.* **1976**, *61*, 31−84.
(2) Lewis, N. S. *Annu. Rev. Phys. Chem.* **1991**, *42*, 543−580.
(3) Miller, R. J. D.; McLendon, G. L.; Nozik, A. J.; Schmickler, W.; Willig, F. *Surface Electron Transfer Processes*; VCH Publishers: New York, 1995; pp 167−309.
(4) Memming, R. *Semiconductor Electrochemistry*; Wiley-VCH Verlag: Weinheim, Germany, 2001; pp 300−331.
(5) Tani, T. *Photographic Sensitivity*; Oxford University Press: New York, 1995.
(6) O'Regan, B.; Grätzel, M. *Nature* **1991**, *353*, 737−740.
(7) Nazeeruddin, M. K.; Kay, A.; Rodicio, I.; Humphry-Baker, R.; Müller, E.; Liska, P.; Vlachopoulos, N.; Grätzel, M. *J. Am. Chem. Soc.* **1993**, *115*, 6382−6390.
(8) Hagfeldt, A.; Grätzel, M. *Chem. Rev.* **1995**, *95*, 49−68.
(9) Spitler, M. T.; Parkinson, B. A. *Langmuir* **1986**, *2*, 549−553.
(10) Parkinson, B. A. *Langmuir* **1988**, *4*, 967−976.
(11) Kemnitz, K.; Tamai, N.; Yamazaki, I.; Nakashima, N.; Yoshihara, K. *J. Phys. Chem.* **1986**, *90*, 5094−5101.
(12) Kemnitz, K.; Tamai, N.; Yamazaki, I.; Nakashima, N.; Yoshihara, K. *J. Phys. Chem.* **1987**, *91*, 1423−1430.
(13) Wright, J. D. *Molecular Crystals*; 2nd ed.; Cambridge University Press: Cambridge, 1995.
(14) Kobayashi, T., Ed. *J-Aggregates*; World Scientific Publishing: Singapore, 1996.
(15) McRae, E. G.; Kasha, M. *Physical Processes in Radiation Biology*; Augenstein, L., Mason, R., Rosenberg, B., Eds.; Academic Press: New York, 1964; pp 23−42.

Changes in sensitization spectra associated with dye aggregate formation have also been reported in photoelectrochemical studies.[9,10,16,17] However, dye aggregates and defective microcrystallites have often been considered to be unfavorable for dye-sensitized solar cells. The presence of dye aggregates could complicate the fate of photogenerated electron−hole pairs or excitons and the kinetics of the electron-transfer processes.[3] Concentration quenching of the dye excited states could occur via electron trapping by dye aggregates after energy transfer processes such as Förster-type energy transfer or energy hopping.[18,19] This was the explanation for a decrease of the QYAP as the dye concentration within the monolayer was increased on a SnO_2 surface.[17,20] Although dye multilayers have also been utilized for sensitizing semiconductor surfaces,[21−25] three-dimensional dye aggregate structures or microcrystallites had lower quantum yields for electron injection due to low exciton mobilities within the thick dye structures.[23−25] Structurally well-defined epitaxial layers of phthalocyanines were vacuum deposited on SnS_2 to study photosensitization efficiencies and showed relatively high QYAP values (≥10%) at coverages up to several monolayers.[26] However, thicker layers showed a decrease in the QYAP values due to the difficulties associated with carrier transport through the molecular solids.

Scanning probe microscopies provide the opportunity to study the nanoscale structures of dye molecules adsorbed on surfaces. Scanning tunneling microscopy (STM) has been applied to show molecular ordering of vacuum-deposited phthalocyanines[27−30] and perylene derivatives[31,32] on copper, gold, graphite, MoS_2, and silicon surfaces. Cyanine dye J- and H-aggregates were also imaged by STM.[33−36] Atomic force microscopy (AFM) has also been used to investigate phthalocyanine films,[37] cyanine dye J-aggregates,[38−43] and other organic dye aggregates.[44−47] For example, several nanometer thick leaf-like structures of pseudoisocyanine J-aggregates at the mica/water interface have been recently reported.[41−43] However, direct confirmation of the relationship between the morphologies of the dyes on the semiconductor surface and their photosensitizing properties has not been explored. The only study to correlate AFM morphologies, light absorption, and photocurrent spectra was reported for vacuum deposited phthalocyanines on TiO_2 single crystals; however, this study was mostly concerned with thick dye layers and the absorption spectra were recorded on glass slides rather than the actual sensitized substrates.[48]

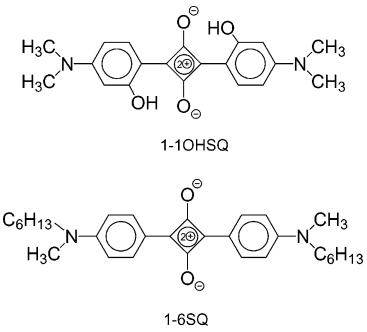

Figure 1. Chemical structures of the dye molecules used: 2,4-bis(4-(*N*,*N*-dimethylamino)-2-hydroxyphenyl)squaraine (1-1OHSQ, upper) and 2,4-bis-(4-(*N*-methyl-N-hexylamino)phenyl)squraine (1-6SQ, lower).

We have shown recently that 2,4-bis(4-(*N*,*N*-dimethylamino)-2-hydroxyphenyl)squaraine (1-1OHSQ, Figure 1)[49] forms at least two distinct morphologies (monolayers and 3D microcrystallites) when it was adsorbed from dichloromethane solutions onto SnS_2 basal plane surfaces with correspondingly different excitation spectra for photocurrent generation in aqueous electrolytes.[50] Squaraine dyes have a donor−acceptor−donor (D−A−D) structure producing a strong absorption band in the visible spectral region. In the solid state, squaraines exhibit a broad absorption spectrum extending into the near-IR region and also exhibit high photoconductivities due to strong intermolecular interactions within the crystal. These attributes make squaraines attractive for use as organic photoconductors in laser printers[51,52] and as nonlinear optical materials.[53−58] Studies

(16) Tributsch, H. *Ber. Bunsen-Ges. Phys. Chem.* **1969**, *73*, 582−590.
(17) Memming, R. *Faraday Discuss. Chem. Soc.* **1974**, *58*, 261−270.
(18) Nakashima, N.; Yoshihara, K.; Willig, F. *J. Chem. Phys.* **1980**, *73*, 3553−3559.
(19) Willig, F.; Blumen, A.; Zumofen, G. *Chem. Phys. Lett.* **1984**, *108*, 222−227.
(20) Miyasaka, T.; Watanabe, T.; Fujishima, A.; Honda, K. *J. Am. Chem. Soc.* **1978**, *100*, 6657−6665.
(21) Jaeger, C. D.; Fan, F.-R. F.; Bard, A. J. *J. Am. Chem. Soc.* **1980**, *102*, 2592−2598.
(22) Giraudeau, A.; Fan, F.-R. F.; Bard, A. J. *J. Am. Chem. Soc.* **1980**, *102*, 5137−5142.
(23) Miyasaka, T.; Watanabe, T.; Fujishima, A.; Honda, K. *Photochem. Photobiol.* **1980**, *32*, 217−222.
(24) Tien, H. T.; Higgins, J. *J. Electrochem. Soc.* **1980**, *127*, 1475−1478.
(25) Yanagi, H.; Chen, S.; Lee, P. A.; Nebesny, K. W.; Armstrong, N. R.; Fujishima, A. *J. Phys. Chem.* **1996**, *100*, 5447−5451.
(26) Chau, L.-K.; Arbour, C.; Collins, G. E.; Nebesny, K. W.; Lee, P. A.; England, C. D.; Armstrong, N. R.; Parkinson, B. A. *J. Phys. Chem.* **1993**, *97*, 2690−2698.
(27) Lippel, P. H.; Wilson, R. J.; Miller, M. D.; Wöll, C.; Chiang, S. *Phys. Rev. Lett.* **1989**, *62*, 171−174.
(28) Ludwig, C.; Strohmaier, R.; Petersen, J.; Gompf, B.; Eisenmenger, W. *J. Vac. Sci. Technol., B* **1994**, *12*, 1963−1966.
(29) Lu, X.; Hipps, K. W.; Wang, X. D.; Mazur, U. *J. Am. Chem. Soc.* **1996**, *118*, 7197−7202.
(30) Chizhov, I.; Scoles, G.; Kahn, A. *Langmuir* **2000**, *16*, 4358−4361.
(31) Ludwig, C.; Gompf, B.; Petersen, J.; Strohmaier, R.; Eisenmenger, W. *Z. Phys. B* **1994**, *93*, 365−373.
(32) Uder, B.; Ludwig, C.; Petersen, J.; Gompf, B.; Eisenmenger, W. *Z. Phys. B* **1995**, *97*, 389−390.
(33) Kawasaki, M.; Ishii, H. *J. Imaging Sci. Technol.* **1995**, *39*, 213−222.
(34) Kawasaki, M.; Sato, T.; Yoshimoto, T. *Langmuir* **2000**, *16*, 5409−5417.
(35) Owens, R. W.; Smith, D. A. *Langmuir* **2000**, *16*, 562−567.
(36) Janssens, G.; Touhari, F.; Gerritsen, J. W.; van Kempen, H.; Callant, P.; Deroover, G.; Vandenbroucke, D. *Chem. Phys. Lett.* **2001**, *344*, 1−6.
(37) Nakamura, M.; Morita, Y.; Mori, Y.; Ishitani, A.; Tokumoto, H. *J. Vac. Sci. Technol., B* **1996**, *14*, 1109−1113.
(38) Wolthaus, L.; Schaper, A.; Möbius, D. *Chem. Phys. Lett.* **1994**, *225*, 322−326.
(39) Higgins, D. A.; Kerimo, J.; Vanden Bout, D. A.; Barbara, P. F. *J. Am. Chem. Soc.* **1996**, *118*, 4049−4058.
(40) Saijo, H.; Shiojiri, M. *J. Imaging Sci. Technol.* **1997**, *41*, 266−271.
(41) Sugiyama, S.; Yao, H.; Matsuoka, O.; Kawabata, R.; Kitamura, N.; Yamamoto, S. *Chem. Lett.* **1999**, 37−38.
(42) Yao, H.; Sugiyama, S.; Kawabata, R.; Ikeda, H.; Matsuoka, O.; Yamamoto, S.; Kitamura, N. *J. Phys. Chem. B* **1999**, *103*, 4452−4456.
(43) Sugiyama Ono, S.; Yao, H.; Matsuoka, O.; Kawabata, R.; Kitamura, N.; Yamamoto, S. *J. Phys. Chem. B* **1999**, *103*, 6909−6912.
(44) Daehne, L.; Tao, J.; Mao, G. *Langmuir* **1998**, *14*, 565−568.
(45) Tao, J.; Mao, G.; Daehne, L. *J. Am. Chem. Soc.* **1999**, *121*, 3475−3485.
(46) Terrettaz, S.; Tachibana, H.; Matsumoto, M. *Langmuir* **1998**, *14*, 7511−7518.
(47) Ricceri, R.; Neto, C.; Abbotto, A.; Facchetti, A.; Pagani, G. A. *Langmuir* **1999**, *15*, 2149−2151.
(48) Taira, S.; Miki, T.; Yanagi, H. *Appl. Surf. Sci.* **1999**, *143*, 23−29.
(49) This dye was erroneously labeled bis(4-(dimethylamino)-dihyroxyphenyl)-squaraine in refs 50 and 64.
(50) Takeda, N.; Parkinson, B. A. *Electrochim. Acta* **2000**, *45*, 4559−4564.
(51) Wingard, R. E. *IEEE Industry Applications* **1982**, 1251−1254.
(52) Law, K.-Y. *Chem. Rev.* **1993**, *93*, 449−486.
(53) Ashwell, G. J.; Jefferies, G.; Hamilton, D. G.; Lynch, D. E.; Roberts, M. P. S.; Bahra, G. S.; Brown, C. R. *Nature* **1995**, *375*, 385−388.
(54) Ashwell, G. J.; Bahra, G. S.; Brown, C. R.; Hamilton, D. G.; Kennard, C. H. L.; Lynch, D. E. *J. Mater. Chem.* **1996**, *6*, 23−26.
(55) Ashwell, G. J.; Wong, G. M. S.; Bucknall, D. G.; Bahra, G. S.; Brown, C. R. *Langmuir* **1997**, *13*, 1629−1633.
(56) Ashwell, G. J.; Williamson, P. C.; Green, A.; Bahra, G. S.; Brown, C. R. *Aust. J. Chem.* **1998**, *51*, 599−604.
(57) Ashwell, G. J.; Jefferies, G.; Rees, N. D.; Williamson, P. C.; Bahra, G. S.; Brown, C. R. *Langmuir* **1998**, *14*, 2850−2856.
(58) Meyers, F.; Chen, C.-T.; Marder, S. R.; Brédas, J.-L. *Chem.—Eur. J.* **1997**, *3*, 530−537.

concerning the application of squaraines for photovoltaic cells and photosensitizers for semiconductors were also reported, but the efficiencies measured in these studies were rather low.[59−61] Recent STM studies from our laboratory on a family of squaraines with various alkyl chain lengths revealed highly ordered structures on highly oriented pyrolytic graphite (HOPG) surfaces with many of the molecules exhibiting several different 2D polymorphs.[62,63] We also discovered a large hysteresis and electrolyte anion dependent peak potentials in cyclic voltammograms of squaraine layers on HOPG, associated with the formation of ordered aggregates.[64] Together with these findings, further studies on the morphologies of squaraine dye molecules and their photosensitization properties should reveal interesting insights into the structure−property relationships of the dye sensitization process. SnS_2 single-crystal surfaces are an excellent choice for the purposes of this study. Tin disulfide (E_g = 2.2 eV) has a layered structure, and cleaved surfaces exhibit many square micron areas of atomically flat van der Waals (0001) surfaces, making it an ideal platform for AFM studies of adsorbates. The absence of surface states associated with dangling bonds, that could act as recombination centers for photoinjected electrons, makes SnS_2 a model system for dye sensitization studies and also contributes to the high quantum yields mentioned previously. In this study, we also employ a squaraine with a longer alkyl chain, specifically 2,4-bis(4-(*N*-methyl-*N*-hexylamino)phenyl)squaraine (1-6SQ), and compare its behavior with that of 1-1OHSQ. The structures of these two dyes are shown in Figure 1. Absorption spectra of the squaraine dye on SnS_2 surface were not measured in our previous study[50] but herein are compared with their morphologies obtained by AFM and their photocurrent quantum yield both per incident (QYIP) and per absorbed (QYAP) photon values.

Experimental Section

Materials. One of the dyes 2,4-bis(4-(*N*,*N*-dimethylamino)-2-hydroxyphenyl)squaraine (1-1OHSQ) was a gift from Lexmark International Corporation and used as received. Another squaraine dye 2,4-bis(4-(*N*-methyl-*N*-hexylamino)phenyl)squraine (1-6SQ) was synthesized in Professor Ashwell's group at Cranfield University, UK and also used as received. Tin disulfide single crystals were synthesized by melt−growth (Bridgman) method and were *n*-doped with chlorine.[65] Dichloromethane (Fischer Scientific, spectranalyzed grade), lithium chloride (Fischer Scientific), ruthenium(III) hexamine (Strem Chemicals Inc.), and other chemicals were reagent grade and used as received. Water used was purified with a Millipore Milli-Q water purification system (18 MΩ cm).

Deposition of Squaraine Dyes onto Tin Disulfide Surfaces. Solid squaraine dyes were dissolved in dichloromethane to prepare solutions of the desired concentration. We found that 1-1OHSQ had limited solubility ($\sim 10^{-5}$ mol L^{-1}) in this solvent at room temperature and tended to form precipitates over time. Therefore, small volumes (typically 10 mL) of solution were prepared for each set of experiments, and concentrations were determined spectrophotometrically (λ_{max} = 638 nm, $\epsilon = 3.3 \times 10^5$ M^{-1} cm^{-1}).[66] 1-6SQ had similar spectral properties in dichloromethane (λ_{max} = 635 nm, $\epsilon = 3.4 \times 10^5$ M^{-1} cm^{-1}) but has a much higher solubility. Various concentrations of 1-6SQ solutions were prepared by dilution of a 1 mM stock solution. UV−vis absorption spectra of the prepared dye solutions were measured with either an HP 8452A diode array spectrophotometer or a Cary 500 Scan UV−vis−NIR spectrophotometer (Varian Instruments). A quartz cell with either a 1 mm or a 10 mm optical path length was used. Immediately before use, the dye solutions were filtered through a membrane filter with a pore diameter of 0.02 μm (Whatman Anodisc 13 or Anotop 25 plus) to remove any particulates. Occasionally the dye solutions were sonicated just before dye deposition onto SnS_2 crystals.

Tin disulfide single crystals were cut into thin pieces with a razor blade. Fresh basal planes were exposed by cleaving with adhesive tape (Scotch, 3M). Methods for the deposition of squaraine dyes onto basal planes of SnS_2 were essentially the same as those used in the previous study.[50] One method is dipping a cleaved SnS_2 piece into dye solutions in a closed vial for 2 min and withdrawing vertically to drain excess solution (dipping method). Another method is dropping aliquots of the dye solutions onto the cleaved SnS_2 and allowing the solvent to evaporate in ambient air (dropping method). In some experiments, samples were enclosed in a container with a dichloromethane atmosphere to slow the evaporation rates.

Atomic Force Microscopy (AFM). The morphologies of the deposited squaraine dyes on SnS_2 were investigated using atomic force microscopy. A Nanoscope IIIa scanning probe microscope (Digital Instruments) was operated in tapping mode with either an E or a J scanner. Conical silicon AFM tips (Ultralevers, Park Scientific Instruments) with a nominal spring constant of $\sim$0.26 N m^{-1} or $\sim$0.40 N m^{-1} were used. Dye deposited SnS_2 pieces were fixed onto a circular steel plate (Ted Pella) by applying silver paint (SPI, Flash-Dry Silver Paint) between them and mounted on the AFM piezo cap. All measurements were conducted in ambient air.

Vis−NIR Absorption Spectroscopy of Squaraine Dyes Adsorbed on SnS_2. Electronic absorption spectra of squaraine dyes adsorbed on SnS_2 were measured with a Cary 500 Scan UV−vis−NIR spectrophotometer. Samples were mounted on a solid sample holder with a 5 mm diameter aperture. Measuring the spectrum of a piece of bare SnS_2 before depositing the dyes provided a baseline for the correction of subsequent spectra. A baseline was shifted if necessary to obtain near zero absorbance at $\sim$900 nm. At energies higher than the band gap energy of SnS_2 (λ < 560 nm), the absorption due to SnS_2 was too high and prevented us from measuring the absorbance due to adsorbed dyes. Many absorbance measurements were averaged to obtain a better signal-to-noise ratio. However, optical interference fringes due to the thin SnS_2 samples were sometimes superimposed on the spectra. After measuring the absorption spectra, the samples could be used for AFM and/or photoelectrochemical measurements.

Photoelectrochemical Measurements. Samples were mounted in a reusable electrode holder made of Teflon with screws holding a front plate onto the sample. Electrical contacts were made through copper plate in the back of the holder onto which the samples were fixed with silver paint. The Teflon holder had a circular opening (4 mm diameter) for electrolyte contact. A flat latex gasket was placed between the SnS_2 and front piece of the Teflon holder to help seal the electrolyte from contact with the back contact. A thin layer of vacuum grease (Apiezon N, GEC Alsthom) was used on contacts between two pieces of the Teflon holder to aid sealing.

A Pyrex three-compartment electrochemical cell with a flat window was used to house the working electrode together with a Pt gauze counter electrode and a saturated calomel reference electrode (SCE). Aqueous solutions containing 1 M LiCl were used as the electrolyte. Unless otherwise noted, 10 mM hydroquinone was added to the electrolyte as a regenerator of photooxidized dyes. Electrolytes were

(59) Loutfy, R. O.; Hsiao, C. K.; Kazmaier, P. M. *Photogr. Sci. Eng.* **1983**, *27*, 5−9.
(60) Kamat, P. V.; Hotchandani, S.; de Lind, M.; Thomas, K. G.; Das, S.; Geroge, M. V. *J. Chem. Soc., Faraday Trans.* **1993**, *89*, 2397−2402.
(61) Hotchandani, S.; Das, S.; Thomas, K. G.; George, M. V.; Kamat, P. V. *Res. Chem. Intermed.* **1994**, *20*, 927−938.
(62) Stawasz, M. E.; Sampson, D. L.; Parkinson, B. A. *Langmuir* **2000**, *16*, 2326−2342.
(63) Stawasz, M. E.; Parkinson, B. A., unpublished results.
(64) Takeda, N.; Stawasz, M. E.; Parkinson, B. A. *J. Electroanal. Chem.* **2001**, *498*, 19−33.
(65) Sharp, L. I.; Soltz, D. L.; Parkinson, B. A., in preparation.
(66) Law, K.-Y. *J. Phys. Chem.* **1987**, *91*, 5184−5193.

purged with nitrogen gas for at least 15 min prior to measurements. The apparatus used for measuring photocurrent was similar to that in the previous study.[50] A 50 W tungsten halogen lamp (Osram) or a 500 W xenon arc lamp (Oriel) equipped with a water filter was used as a light source. A Jarrell-Ash MonoSpec 27 monochromator, 2 mm wide slits, a 500 nm short cutoff filter, and a collimating lens were used to select the wavelength and focus the light beam to an ~2 mm × 2 mm rectangular spot on the electrode surface. Potentiostatic control of the electrode potential was done with a Princeton Applied Research 174A polarographic analyzer (EG&G). The light beam was modulated at 28 Hz with a mechanical chopper, and photocurrents were measured using a lock-in technique with an SR830 lock-in amplifier (Stanford Research Systems). An IBM PC was used to control the scanning of the monochromator to obtain photocurrent action spectra. Lamp spectra were obtained using a thermopile that was calibrated with a photodiode detector. Photocurrent−voltage curves were obtained by slowly stepping the bias voltage and measuring the photocurrent at each potential using a lock-in technique. Potential scans were accomplished with a Macintosh computer equipped with a MacLab/4e interface and EChem v.1.5.1 software (AD Instruments). In some experiments, diode lasers (Lasermax Inc., λ_{max} 690 nm and Imatronic Ltd., model LDL175/820/3, λ_{max} 806 nm) were used as light sources. Alignment of the near-IR beam was performed using a Kodak Reflective IR Detection Card. Illumination with the laser beam was made through a pinhole, and various neutral density filters were used to change the intensity.

Mott−Schottky Measurements. Mott−Schottky measurements[67] of the *n*-doped SnS_2 electrodes were conducted in 1 M LiCl aqueous electrolytes at room temperature to determine the flat band potential (E_{fb}) and dopant density (N_D). Edges of cleaved SnS_2 pieces were sealed with silicone rubber sealant to expose a 0.3 cm^2 electrode area. A Princeton Applied Research 173 potentiostat was combined with an SR830 lock-in amplifier. Capacitance measurements between electrode potentials of 0 and +1.5 V versus SCE with 50 mV increments were performed with various ac modulation frequencies between 2 and 20 kHz (rms amplitude 4 mV). A series RC equivalent circuit was assumed for analysis of data. E_{fb} was deduced from extrapolation of linear parts of plots (> +0.5 V vs SCE). A dielectric constant of 17.7 for SnS_2 was used for the estimation of N_D.[68]

Results and Discussion

Energetics of the Dye/Semiconductor Interface. To determine the feasibility of photosensitization and understand the quantum yields of sensitization for dyes adsorbed onto a semiconductor surface, the relative energy positions of the semiconductor energy bands and the dye's ground and excited states need to be determined.[1,3] The flatband potentials (E_{fb}) of *n*-SnS_2 crystals used in this study were determined via Mott−Schottky measurements to be 0.0 ± 0.1 V versus SCE in the 1 M LiCl aqueous electrolyte. In addition, the slope of the Mott−Schottky plot yielded a dopant density (N_D) of 7 × 10^{16} cm^{-3}, consistent with a value determined from Hall effect measurements (N_D = 7.3 × 10^{16} cm^{-3})[65] on parts of the same crystal. Modulation frequencies in Mott−Schottky measurements, in the range of 2 kHz to 20 kHz did not affect these values beyond the experimental uncertainties.

The formal potentials for the first oxidation of 1-1OHSQ and 1-6SQ measured in dichloromethane are about +0.52 V versus SCE[69] and +0.48 V versus SCE,[70] respectively. Although these potentials may not be completely relevant to a surface confined dye in contact with an aqueous solution, the following experimental results suggest that they are similar. Photosensitization experiments usually use a regenerator (reducing agent) added to the solution to reduce the adsorbed photooxidized dye after it has injected an electron into the conduction band of the semiconductor. We have previously reported anodic photocurrent generation from 1-1OHSQ dyes adsorbed on SnS_2 in 1 M LiCl aqueous electrolyte with 10 mM hydroquinone (H_2Q) under a positive bias.[50] Herein, the effect of the redox potential and chemical identity of the regenerator was investigated using 10 mM concentrations of different reducing agents H_2Q ($E^{\circ\prime}$(Q/H_2Q) = +0.044 V versus SCE at pH 7),[71] $K_4Fe(CN)_6$ ($E^{\circ\prime}$(Fe$(CN)_6^{3-}$/Fe$(CN)_6^{4-}$) = +0.12 V versus SCE),[72] and KI ($E^{\circ\prime}$-(I_3^-/I^-) = +0.30 V versus SCE)[73] added to the 1 M LiCl electrolyte (Figure 2). Photocurrents measured at +0.7 V versus SCE were converted to quantum yield per incident photon (QYIP). Photocurrent action spectra for unsensitized SnS_2 were similar regardless of the presence of the reducing agents (Figure 2, solid curve) except for an increased sub-bandgap response when H_2Q was used (Figure 2, dotted curve). On the other hand, photocurrents were significantly influenced by the reducing agents when SnS_2 electrodes were sensitized with 1-1OHSQ dye (1 × 10^{-10} mol cm^{-2}, prepared by the dropping method). The QYIP was higher with reducing agents with more negative potentials: H_2Q (circles) ≈ ferrocyanide (squares) > iodide (triangles) > no added regenerator (diamonds). These results imply that the recombination reactions are competitive with the dye regeneration process in the present system and that iodide has too positive a redox potential for efficient regeneration. Although the photocurrent−voltage curve showed a less positive

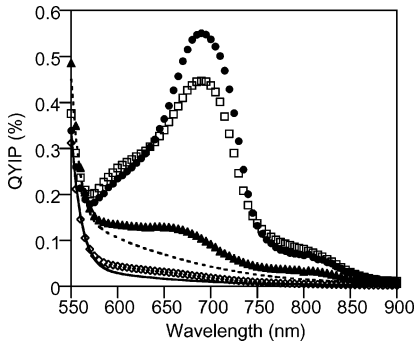

Figure 2. Photocurrent action spectra obtained at +0.7 V vs SCE for SnS_2 electrodes sensitized with ~1 × 10^{-10} mol cm^{-2} 1-1OHSQ prepared by the dropping method. The aqueous 1 M LiCl electrolyte contained 10 mM of various reducing agents: hydroquinone (●), potassium ferrocyanide (□), potassium iodide (▲), and without adding a reducing agent (◇). Spectra obtained for unsensitized (bare) SnS_2 electrodes measured in electrolytes containing 10 mM hydroquinone (dotted curve) and without adding reducing agent (solid curve).

(67) Morrison, S. R. *Electrochemistry at Semiconductors and Oxidized Metal Electrodes*; Plenum Press: New York, 1980.
(68) Lucovsky, G.; Mikkelsen, J. C., Jr.; Liang, W. Y.; White, R. M.; Martin, R. M. *Phys. Rev. B* **1976**, *14*, 1663−1669.
(69) (a) converted from the value reported in ref 69b (+0.41 V vs Ag/AgCl) using the reduction potential of TCNQ internal reference (−0.14 V vs Ag/AgCl). The potential was corrected to SCE using the half-wave potential in 1,2-dichloroethane ($E_{1/2}$(TCNQ/TCNQ$^{\bullet-}$) = +0.212 V vs SHE) reported in the literature (Cheng, Y.; Schiffrin, D. J. *J. Chem. Soc., Faraday Trans.* **1994**, *90*, 2571−2523.) (b) Law, K.-Y.; Facci, J. S.; Bailey, F. C.; Yanus, J. F. *J. Imaging Sci.* **1990**, *34*, 31.
(70) Takeda, N.; Parkinson, B. A., unpublished results.
(71) (a) extrapolated from the standard potential given in ref 71b assuming the potential change of 59 mV/unit pH. (b) Clark, W. M. *Oxidation−Reduction Potentials of Organic Systems*; The Williams & Wilkins Company: Baltimore, MD, 1960; Chapter 14.
(72) Heusler, K. E. *Encyclopedia of Electrochemistry of the Elements*; Bard, A. J., Ed.; Marcel Dekker: New York, 1982; Vol. IX Part A, pp 229−381.
(73) Desideri, P. G.; Lepri, L.; Heimler, D. *Encyclopedia of Electrochemistry of the Elements*; Bard, A. J., Ed.; Marcel Dekker: New York, 1973; Vol. I, pp 91−153.

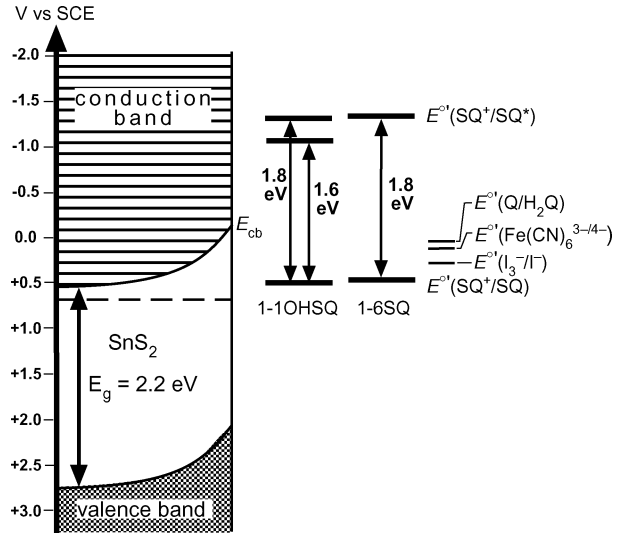

Figure 3. Energy diagram for squaraine dyes (1-1OHSQ and 1-6SQ) adsorbed on *n*-SnS_2 electrodes immersed in aqueous electrolyte under positive polarization. The ground-state potentials of squaraines ($E^{\circ\prime}(SQ^+/SQ)$) were taken from values measured in dichloromethane solution which were converted to SCE scale.[69,70] The peak excitation energy of photocurrent action spectra (1.8 eV) was used to estimate the excited-state potentials of squaraines ($E^{\circ\prime}(SQ^+/SQ^*)$). Redox potentials of reducing agents are also shown. A lower transition energy (1.6 eV) for 3D crystallites of 1-1OHSQ could result in a slightly lower excited-state potential. An approximate position for the conduction band edge of SnS_2 (E_{cb}) is based on the measured flatband potential of bare SnS_2 ($E_{fb} \approx 0.0$ V vs SCE).

onset potential with $Fe(CN)_6^{4-}$, which might be related to faster regeneration kinetics, H_2Q was chosen to be the regenerator for the rest of the experiments reported herein.

In an earlier electrochemical study, we showed that potentials for the oxidation and rereduction of 1-1OHSQ dye layers adsorbed on HOPG electrodes depended on the identity and concentration of the electrolyte anions.[64] If this is also the case on an SnS_2 substrate, the recombination rate of photoinjected electrons would be affected and influence the observed photocurrent quantum yield. However, changing the supporting electrolyte from LiCl to NaBr, NaI, or Na_2SO_4 (1 M), all with 10mM H_2Q used as the regenerator, had no strong effect on the quantum yield and shape of the photocurrent−voltage curves. This result can be understood if one considers the differences between the redox processes in the two cases. In the HOPG study, the redox potentials of the surface-confined dye layers were influenced because of anion incorporation into and expulsion from the dye layers that was necessary to maintain electrical neutrality in the film when large areas of dye molecules were oxidized or rereduced.[64] On the other hand, the photoelectrochemical oxidation process involves only individual dye molecules at any given time and the rapid regeneration reaction makes the lifetime of the oxidized dye very short. In addition, the migration of the photogenerated hole in the dye layer to a more stable site is also possible. Ion pairing of oxidized squaraine dyes with electrolyte anions seems weak in the present system, and the ground state potential is not significantly affected.

The energetics of the present dye sensitization system is illustrated in Figure 3 based on the assumption that the dye oxidation potential is not shifted from values measured in dichloromethane solutions. The 0−0 transition energies were approximated by the peak excitation energy of the photocurrent spectra. Within the uncertainties of the estimation of dye oxidation potentials, the two squaraine dyes studied herein have similar energy levels. Considering that the conduction band edge (E_{cb}) is separated by a few tenths of a volt from E_{fb} for moderately *n*-doped SnS_2, we find that the excited states of squaraines lie well above E_{cb} (0.9−1.2 eV), ensuring fast injection of excited electrons. On the other hand, the ground-state dye energy levels are located about 0.6−0.7 eV below E_{cb}. A threshold of dye oxidation potential was previously observed at ∼0.7 V positive of E_{cb} for monomeric dyes, above which high QYIP values were obtained.[10] The competition between the recombination and regeneration reactions could be easily shifted due to the comparable driving force for the two processes.

Morphology of 1-1OHSQ on SnS_2. STM observations of 1-1OHSQ deposited on HOPG substrate revealed row structures in which adjacent molecules offset each other so that an anilino moiety (donor) and central square ring (acceptor) interact.[62,64] We were unable to image the squaraine molecules with STM on SnS_2 surfaces due to both the incompatibility of the biases needed to image squaraines with the band positions of the SnS_2[62] and the strong interaction of the STM tip with the SnS_2 surface resulting in etching of the surface.[74] In the present study, morphologies of squaraine dyes on SnS_2 surfaces were studied using AFM. Figure 4 shows an example of AFM images obtained for 1-1OHSQ dyes deposited on an SnS_2 surface by the dipping method (images a and b) and by the dropping method (images c and d). Although the geometrical shapes varied from experiment to experiment, we will categorize them into two distinct morphologies, flat islands (2−6 Å high) and 3D crystallites (>7 Å high), as described in the previous paper.[50] Flat islands were considered to consist of ordered layers of flat-lying 1-1OHSQ molecules. Figure 4a shows such islands (2−4 Å thick) on top of nearly complete monolayers (∼2 Å thick). On the other hand, the 3D crystallites were considered to be multilayers of 1-1OHSQ aggregates that frequently had a needlelike shape, as shown in Figure 4b and c. In Figure 4b, step edges of SnS_2 can be also seen. The observed morphologies were influenced by the preparation method. The dipping method was more likely to produce flat islands, while the 3D crystallites were grown more frequently by the dropping method. However, we consider that every sample may have regions with both morphologies, since we occasionally observed 3D crystallites for the dipping method (Figure 4b) and flat islands for the dropping method (Figure 4d). A variety of conditions including defect site density on SnS_2, distribution of the dye solution on the surface, and the evaporation rate of solvent, none of which we fully controlled, would influence the nucleation−growth process for the formation of the squaraine morphologies on the surface.[50] In fact, when the evaporation rate was retarded in a closed container by the presence of dichloromethane vapor, AFM images revealed further growth of 3D aggregates. The ambiguity of the morphologies also seems to be influenced by the limited solubility of 1-1OHSQ in dichloromethane that reaches saturation at concentrations of around 15−20 μM. The adsorption/desorption process in both preparation methods is then near a critical point where nucleation rates will control the island formation and thus the coverage.

(74) Parkinson, B. *J. Am. Chem. Soc.* **1990**, *112*, 7498−7502.

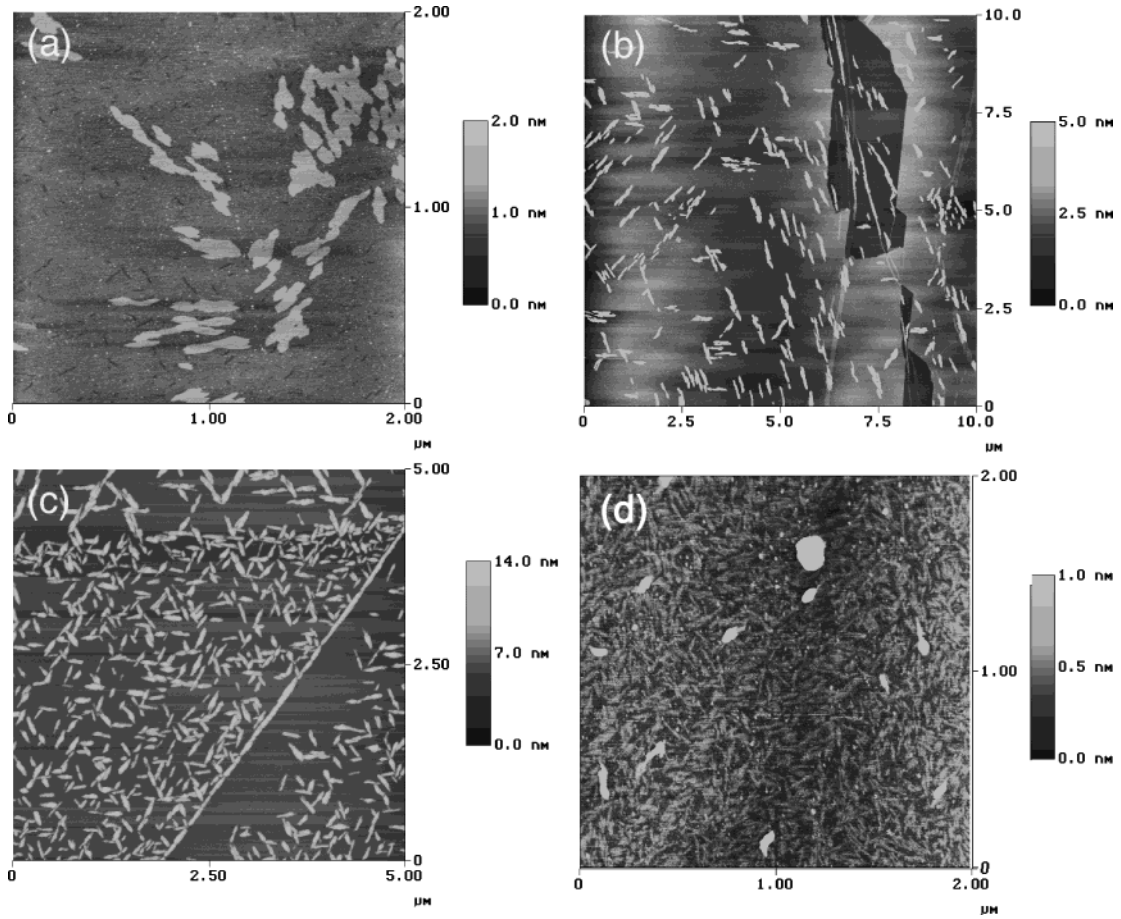

Figure 4. AFM images obtained for 1-1OHSQ adsorbed on SnS_2. Deposition was performed by dipping an SnS_2 piece in an 8 μM 1-1OHSQ solution (in dichloromethane) for 2 min (a and b) or by dropping dichloromethane solution containing $\sim 1 \times 10^{-10}$ mol cm^{-2} equiv of 1-1OHSQ on SnS_2 followed by solvent evaporation (c and d).

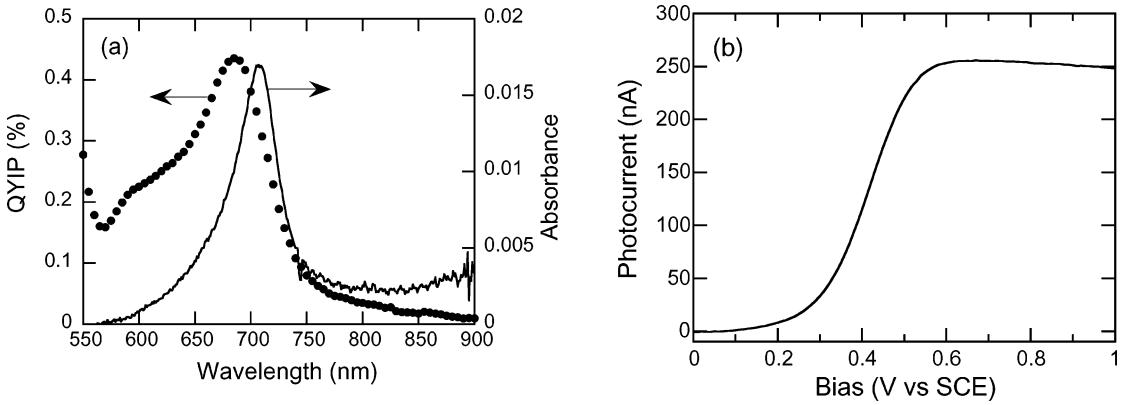

Figure 5. (a) Vis−NIR absorption spectrum (solid curve) and photocurrent action spectrum obtained at a +0.7 V vs SCE bias (●) for 1-1OHSQ on SnS_2 prepared by the dipping method (8 μM for 2 min). Note that the absorption spectrum contains contributions from adsorbates on both sides of the SnS_2 surface. (b) Photocurrent−voltage curve of the sample illuminated at 680 nm (104 μW).

Light Absorption by Adsorbed 1-1OHSQ Dyes. Solid curves in Figures 5a and 6a show two types of solid-state absorption spectra obtained for 1-1OHSQ dyes adsorbed on SnS_2. A sample prepared by the dipping method had an absorption maximum around 710 nm (Figure 5a), assigned to flat-lying 1-1OHSQ molecules. The observed peak was red-shifted ($\Delta E \approx 0.2$ eV) from the dichloromethane solution spectrum ($\lambda_{max} = 638$ nm), suggesting the existence of an electronic interaction between excited dye molecules and conduction band states of SnS_2 and/or an effect of aggregation where transition dipole interactions between even the flat lying dye molecules reduce the excitation energy. On the other hand, a sample prepared by the dropping method (Figure 6a) produced an additional absorption shoulder around 760−800 nm that was associated with the more frequent observation of 3D crystallites in AFM images. As previously reported for photocurrent spectra,[50] this additional band is attributed to intermolecular donor−acceptor charge transfer within 1-1OHSQ crystallites with J-aggregate interactions between the molecules.

Irreproducibility of the dye coverage, as measured by the absorbance of the surface film, was especially apparent when the dipping method was used. Figure 7 shows plots of peak

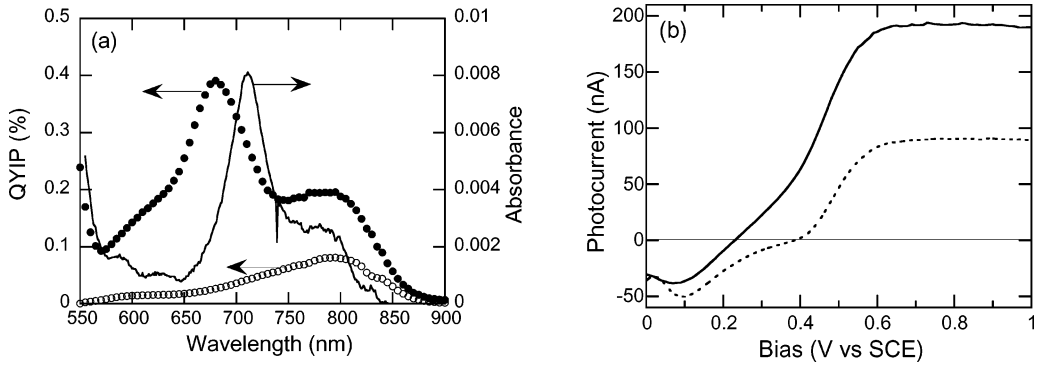

Figure 6. (a) Vis−NIR absorption spectrum (solid curve) and photocurrent action spectrum obtained at +0.7 V (●, anodic photocurrent) and at +0.1 V vs SCE (○, cathodic photocurrent) for 1-1OHSQ on SnS_2 prepared by the dropping method (1×10^{-10} mol cm^{-2}). (b) Photocurrent−voltage curve of the sample illuminated at 680 nm (solid curve, 120 μW) and at 800 nm (dotted curve, 64 μW). A negative sign of the photocurrent refers to a cathodic process.

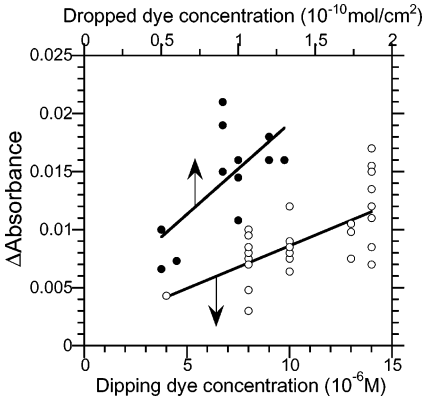

Figure 7. Photoabsorption of 1-1OHSQ adsorbed on SnS_2 against dye solution concentration for the dipping method (○) and dye surface concentration for the dropping method (●). Combined peak absorbance at around 710 and 780 nm bands taken from solid-state vis−NIR spectra in air. Absorbance values for the dipping method were divided by two to account for a single dye/semiconductor interface (refer to text for details).

absorbance versus dye concentration for a number of samples prepared for which the values at the absorbance maxima of ~710 and 780 nm bands were combined to account for the two types of aggregates described previously. The measured absorbance values were divided by two when the dipping method was used to account for a single dye/semiconductor interface, since the adsorbed dyes on both SnS_2 surfaces contribute to the measurements. The averaged values may have as much as a ±50% error due to the possibility of an uneven distribution of dye on the two sides. There is considerable scatter of the absorbance data among different samples that is probably due to the variations in nucleation and growth of the dye layers between the different experiments as discussed previously. A complete monolayer of 1-1OHSQ ($(0.7-1) \times 10^{-10}$ mol cm^{-2} as measured by STM)[64] would have a peak absorbance of 0.007−0.01, provided it has the same absorptivity as will be shown for 1-6SQ films. Since both flat islands and 3D aggregates would contribute to the measured absorbance shown in Figure 7, varying populations of two aggregate forms among samples could also contribute to scatter in the data especially for the dropping method (closed circles) if the two dye forms had different absorption coefficients. Nevertheless, flat islands prepared by the dipping method (open circles) are more likely to have similar absorptivities as 1-6SQ and data in Figure 7, and AFM images indicate that dipping in an 8−10 μM solution gives a near one monolayer coverage of 1-1OHSQ.

Photosensitization Efficiency of 1-1OHSQ. The irregularities observed for dye morphologies and coverage make the comparison of three measurements (AFM, absorption spectrum, and photocurrent spectrum) more difficult because the AFM gives only very local information and the latter two techniques provide spatially averaged information. To reduce the uncertainty, absorbance and photocurrent yields were compared for the same sample to deduce quantum yield per absorbed photon (QYAP) values. Figure 5a shows such a comparison for an SnS_2 electrode sensitized by 1-1OHSQ with a mostly flat island morphology. A photocurrent action spectrum taken at +0.7 V versus SCE (Figure 5a, circles) had a single peak at around 685 nm that was slightly blue-shifted from the absorption spectrum (solid curve) measured in air. This shift is explained by the effect of the higher dielectric constant of an aqueous electrolyte influencing the $\pi-\pi^*$ transition energy of squaraines.[75,76] Using the average peak absorbance, a QYAP value for the photocurrent peak in Figure 5a is calculated to be 23%. QYAP values at +0.7 V versus SCE ranged from 15 to 40% for a number of samples prepared by the dipping method with 0.3−1 monolayer coverages of 1-1OHSQ and showing a photocurrent peak around 680−690 nm.

The photocurrent−voltage curve measured with 680 nm incident light (104 μW, Figure 5b) shows the onset of an anodic photocurrent at 0.1 to 0.2 V more positive than the E_{fb} of bare SnS_2 electrodes. The photocurrent increased as the positive bias increased and leveled off around +0.55 V versus SCE. This typical behavior is due to the competition between the escape of injected electrons and recombination reactions with oxidized dyes.[10,77,78] In the absence of recombination, the photocurrent−voltage curve would be nernstian and reach a plateau value within 100 mV of its onset. Photocurrents obtained at the plateau region indicate that around three-quarters of the photoexcited dyes did not contribute to photocurrent generation even at these biases. Possible mechanisms for the recombination losses will be discussed later.

Figure 6 presents photocurrent data for an SnS_2 electrode sensitized by the dropping method (~1×10^{-10} mol cm^{-2}) that showed behavior unique to the 3D crystallites of 1-1OHSQ. The photocurrent action spectrum taken at +0.7 V versus SCE (Figure 6a, solid circles) shows two peaks at 680 nm and

(75) Tristani-Kendra, M.; Eckhardt, C. J. *J. Chem. Phys.* **1984**, *81*, 1160−1173.
(76) Bigelow, R. W.; Freund, H.-J. *Chem. Phys.* **1986**, *107*, 159−174.
(77) Spitler, M. T. *J. Electroanal. Chem.* **1987**, *228*, 69−76.
(78) Parkinson, B. A.; Spitler, M. T. *Electrochim. Acta* **1992**, *37*, 943−948.

790−800 nm corresponding to the two peaks observed in the absorption spectrum (solid curve). The emergence of the near-IR band is similar to what was reported in our previous paper where it was assigned to an intermolecular transition between adjacent squaraine chromophores within the 3D crystallites.[50] The 680 nm photocurrent peak was blue-shifted from the absorption spectrum in air as in Figure 5a, but the near-IR response was not. Most likely the majority of the molecules responsible for this peak are in the interior of the 3D crystallites and have very little electrostatic interaction with the electrolyte. QYAP values for each of the photocurrent peaks are calculated to be 22% (680 nm) and 31% (790 nm) using the peak absorbances at 710 and 790 nm, respectively. The latter QYAP value obtained for the near-IR band of 3D crystallites is comparable to those observed for the monolayer thick flat islands. This result implies that exciton migration within these several nanometer thick crystallites is fairly efficient. Photocurrents measured with diode laser illumination at 690 or 806 nm linearly increased with an increase of the incident photon flux to at least ∼0.6 mW of incident power, indicating the regeneration of photooxidized molecules in both types of dye aggregates could keep up with an increased photocarrier generation rate.

When the sensitized electrode containing the 3D aggregates was polarized to less positive potentials, *cathodic* photocurrents were produced. A cathodic photocurrent action spectrum taken at +0.1V versus SCE (open circles in Figure 6a) shows a main peak at around 790−800 nm. Since cathodic photocurrents were not observed for the flat islands such as those shown in Figure 4a, they are exclusively associated with the excitation of 3D crystallites. On the other hand, the anodic photocurrent spectrum is a superposition of both forms of 1-1OHSQ aggregates. Photocurrent−voltage curves measured at two different excitation wavelengths (Figure 6b) illustrate the current inversion associated with the 3D crystallites. Under 800 nm illumination (64 μW, dotted curve), the photocurrent switches direction at around +0.4 V versus SCE, above which 3D crystallites show normal sensitization behavior. On the other hand, the zero current crossing potential is shifted to more negative values (∼+0.2 V versus SCE) under 680 nm illumination (120 μW, solid curve) presumably due to the contribution from the coexisting 1-1OHSQ flat islands. Cathodic photocurrent generation was reported for particulates of squaraine dyes embedded in a polymer film formed on SnO_2 electrodes.[59] This process is also related to observations by Bard and others on phthalocyanine films.[21,22,25] They proposed that benzoquinone, formed by oxidation of hydroquinone, acts as an electron acceptor. It is likely that a potential drop is developed within the 3D crystallites at less positive potentials such that excitons move toward the dye/electrolyte interface and reduce redox species (e.g., benzoquinone) while hole injection into SnS_2 occurs through exciton dissociation and recombination through the channel that competes with anodic photocurrent generation. Changes in photocurrent action spectra (e.g., changes in relative QYIP of the two bands) were occasionally observed after photocurrent−voltage measurements. Application of a more positive potential could cause structural changes in the dye multilayer by photooxidation or dark oxidation.

Morphology of 1-6SQ on SnS_2. In contrast to 1-1OHSQ, the morphologies of 1-6SQ molecules on an SnS_2 substrate were not greatly affected by the preparation method. The higher solubility of 1-6SQ in dichloromethane would make conditions for the adsorption/desorption processes similar for both the dipping and the dropping methods. Accordingly, sensitization experiments with 1-6SQ on SnS_2 photoelectrodes prepared by the two methods showed similar behavior. Figure 8 shows AFM images obtained for different coverages of 1-6SQ prepared by the dropping method. At a coverage of 0.5×10^{-10} mol cm^{-2}, flat two-dimensional layers of 1-6SQ dye form large domains with occasional voids (typically 2−4 Å deep) appearing as dark areas in the AFM image (Figure 8a). At a coverage of 1×10^{-10} mol cm^{-2}, domains became denser and many of the pits display a linear shape oriented along directions ∼60° or ∼120° to each other (Figure 8b), much like the orientations of the 3D aggregates in Figure 4. Higher resolution STM studies of the molecular arrangement of 1-6SQ on HOPG surfaces showed that the molecules form row structures similar to 1-1OHSQ on this van der Waals surface with a packing density of $\sim 1 \times 10^{-10}$ mol cm^{-2}.[63] The HOPG 2D structure shows interdigitation of the hydrocarbon tails with those of neighboring rows of molecules resulting in similar or even higher packing densities than those for 1-1OHSQ. We assume that the structure on the van der Waals surface of SnS_2 is similar, since only one polytype was observed on HOPG surfaces and there was no commensuration with the HOPG substrate that would make the structure unique to this substrate.[63]

As the dye concentration was increased to 2×10^{-10} mol cm^{-2}, agglomerated structures (>1 nm high) appeared as bright spots on top of the flat layers in the AFM images (Figure 8c). At even higher concentrations (9×10^{-10} mol cm^{-2}), 3D aggregates with several nanometer to ∼20 nm vertical heights became predominant (Figure 8d). It is apparent that 1-6SQ on SnS_2 forms flat-lying island structures at low coverage and 3D aggregates at higher coverage regardless of the preparation method employed in this study. Therefore, the dropping method is preferred, since the amount of dye added to the surface is known and the problem of adsorption on both sides of the crystal is eliminated.

Photoabsorptivity and Spectral Shift of 1-6SQ Layers. The dye coverage dependence for 1-6SQ was clearly seen in its visible−NIR absorption spectra. Figure 9 shows there is a linear dependence of the peak absorbance on dye surface concentration for the dropping method (closed symbol) and solution concentrations for the dipping method (open symbol). Again, the absorbance values were divided by two when the dipping method was used. From the plots for the dropping method, one would expect an absorptivity of $\sim 0.010 \pm 0.002$ per dye coverage of 1×10^{-10} mol^{-1} cm^{-2}, corresponding to a close-packed monolayer as revealed by STM.[63] This relationship could be used to estimate dye surface coverages for the dipping method from its absorbance value as well and was used previously to estimate 1-1OHSQ coverages.

The solid curve in Figure 10a shows an absorption spectrum for 1-6SQ on SnS_2 prepared by dipping it into a 10 μM dye solution. The dye coverage is estimated to be about 0.4 monolayer using the relationship found in Figure 9. The peak at around 640 nm is almost identical to the solution spectrum in dichloromethane (dotted curve, $\lambda_{max} = 635$ nm). This is different from the 1-1OHSQ behavior where a >0.1 eV lowering

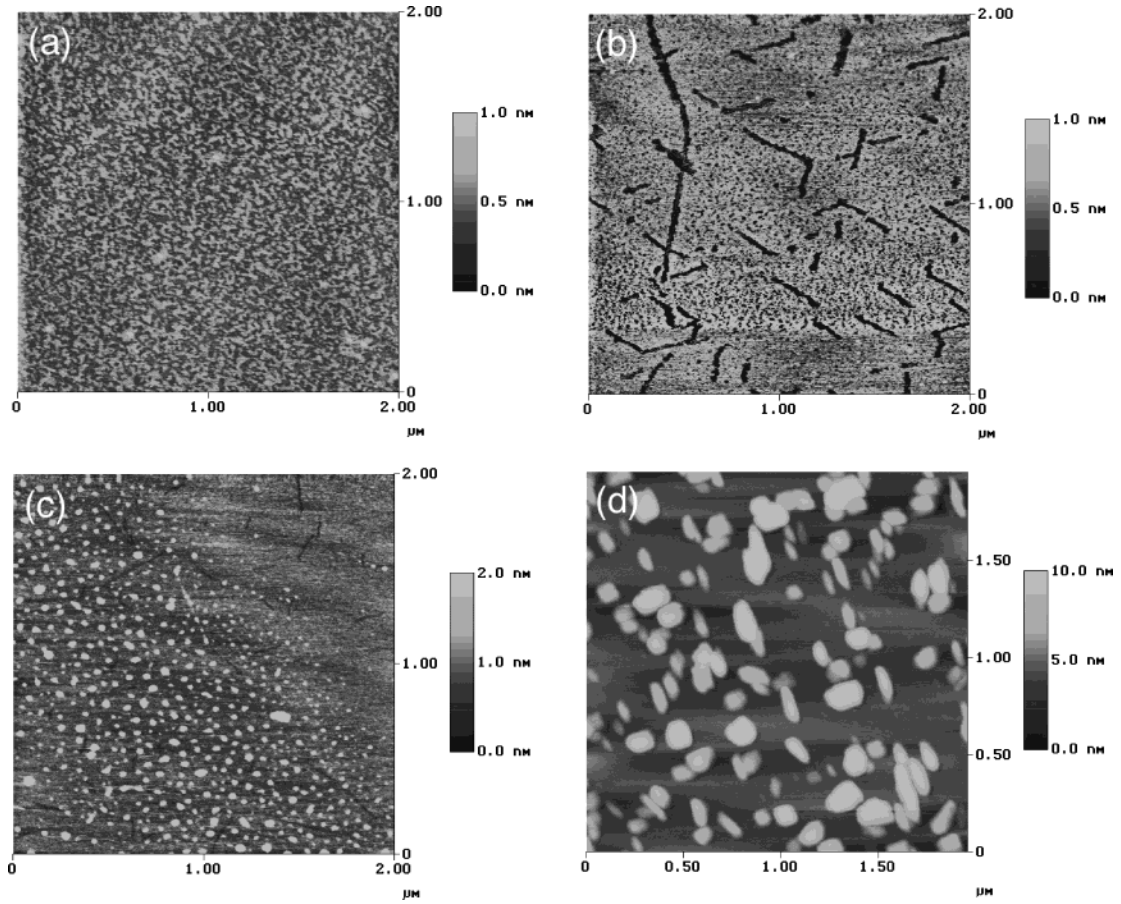

Figure 8. AFM images (2×2 μm^2) obtained for 1-6SQ adsorbed on SnS_2. Deposition was performed by dropping a dye solution in dichloromethane followed by solvent evaporation in ambient air. Surface dye concentrations of 0.5×10^{-10} (a), 1.0×10^{-10} (b), 2.0×10^{-10} (c), and 8.7×10^{-10} (d) mol cm^{-2}.

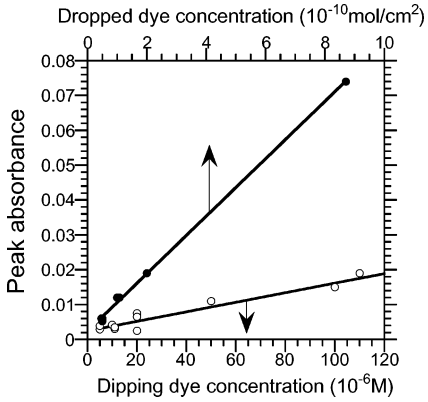

Figure 9. Photoabsorption of 1-6SQ adsorbed on SnS_2 against dye solution concentration for the dipping method (○) and dye surface concentration for the dropping method (●). Peak absorbance values were obtained from the solid-state vis−NIR spectra measured in air. Data for the dipping method were divided by two to account for single dye/semiconductor interface (refer to text for details).

of the transition energy was observed for similar dye coverage. The lack of a red shift suggests a weaker electronic interaction between 1-6SQ and the SnS_2 substrate. On the other hand, a red shift was observed at higher dye coverages of 1-6SQ. This is illustrated by absorption spectra obtained for dye coverages of 0.5, 1.0, and 2.0×10^{-10} mol cm^{-2} (solid curves in Figure 11a). The molecules lie flat on the surface at less than one monolayer coverage, as was seen in the AFM images and the STM images on HOPG, resulting in a spectrum indicative of a monomer (curve a), very much like the solution spectrum. At higher surface coverages, 1-6SQ molecules may start to tilt up from the surface, allowing intermolecular transitions similar to the 3D aggregates of 1-1OHSQ (curves b and c). Three-dimensional aggregates of 1-6SQ found in the AFM images are formed from these interactions. However, the reduction of the excitation energy (ΔE 0.14−0.17 eV) deduced from spectral shift for 1-6SQ (λ_{max} from ∼640 to 690−700 nm) was slightly smaller than the shift observed for 1-1OHSQ 3D crystallites (ΔE 0.16−0.2 eV, λ_{max} from 710 to 780−800 nm). The linear dependence of the peak absorption shown in Figure 9 indicates that the absorptivity is nearly constant throughout these changes. The absorption band found at 690−700 nm resembles the absorption spectrum of aggregates observed in an L-B film of 1-6SQ that showed surprisingly efficient second harmonic generation (SHG).[53] The authors of that study also attributed this band to an intermolecular transition. Moreover, we have observed a similar structure in STM images of one polytype of 18-18SQ (similar to 1-6SQ but with four octadecyl groups attached to the nitrogens) adsorbed onto HOPG.[63]

Photosensitization Behavior of 1-6SQ. While the spectral change was observed in the solid-state absorption spectra, the sensitized photocurrent peak measured at +0.7 V versus SCE in aqueous electrolyte remained constant at around 690 nm (Figures 10 and 11). This spectral difference between absorption and sensitization spectra seen at low coverage may seem unusual, but it can be explained if the electrolyte induces a

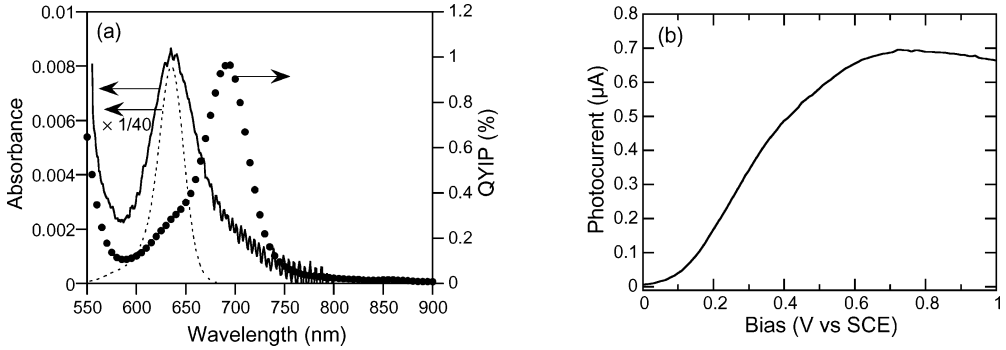

Figure 10. (a) Vis−NIR absorption spectrum (solid curve) and photocurrent action spectrum obtained at a +0.7 V vs SCE bias (●) for 1-6SQ on SnS_2 prepared by the dipping method (10 μM). Absorption spectrum of a 10 μM 1-6SQ solution in dichloromethane (dotted curve, 1 mm path length, $^1/_{40}$ scale) is shown for comparison. (b) Photocurrent−voltage curve of the sample illuminated at 690 nm (130 μW).

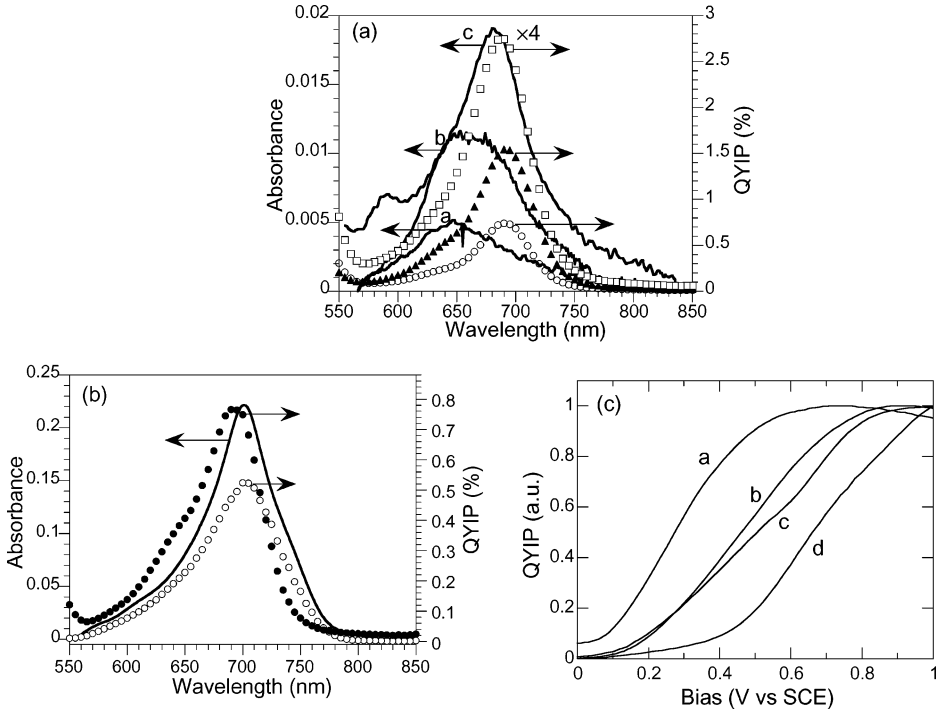

Figure 11. (a) Vis−NIR absorption spectra (curves a−c) and corresponding photocurrent action spectra (bias at +0.7 V vs SCE) for 0.5 × 10^{-10} (○), 1.0 × 10^{-10} (▲), and 2.0 × 10^{-10} mol cm^{-2} (□) of 1-6SQ on SnS_2 prepared by the dropping method. (b) Vis−NIR absorption spectrum (solid curve) and photocurrent action spectrum at +0.7 V vs SCE (●) for 1-6SQ on SnS_2 prepared by the dipping method (1 mM). Cathodic photocurrents were observed prior to application of more positive biases (○, measured at 0.0 V vs SCE). (c) Photocurrent−voltage curves of 1-6SQ on SnS_2 prepared by dropping 0.5 (curve a), 1.0 (curve b), and 2.0 (curve c) × 10^{-10} mol cm^{-2} and dipping in 1mM solution (curve d). Illumination at 690 nm.

similar structural rearrangement as proposed previously for the absorption spectra. We propose that the dye molecules reorient at the interface such that the chromophore goes from lying on the SnS_2 surface to being perpendicular to it while the hydrophobic hexyl chains can still maintain their contact. The resulting change in chromophore interaction, from the surface to direct J-aggregate-like interaction with other squaraines, is then responsible for the spectral shift observed when immersed in electrolytes. Rationalization of this hypothesis can be made considering the hydrophobic nature of these dye molecules. Both squaraine dyes used in this study are insoluble in water, and it is expected that physisorbed dye layers adhere to SnS_2 surfaces in aqueous electrolyte by a hydrophobic interaction[79] in addition to van der Waals forces. A flat-lying configuration, exposing a large area to water, is energetically unfavorable for the orientation of the interfacial water molecules. The tilted structure may be further stabilized by additional donor−acceptor interaction between the chromophores. This was not the case for 1-1OHSQ, since it lacks a long alkyl chain to interact with the SnS_2 while "standing up".

Now we will evaluate the photocurrent yields obtained from the 1-6SQ dye layers. If the absorption peak is shifted in aqueous electrolyte and the absorbance of the dyes participating in photocurrent generation is a half of that measured, the QYIP value of 0.96% at 690 nm shown in Figure 10a corresponds to a QYAP of 97%. Similarly high QYAP values (>60%) were measured at +0.7 V versus SCE for a number of different samples with one monolayer or less coverage of 1-6SQ. The results indicate that essentially all the photons absorbed by 1-6SQ dyes can be converted to photocurrent at a sufficiently positive bias. The achievement of 100% QYAP for dye aggregates can be compared to another high efficiency injection

(79) Israelachvili, J. N. *Intermolecular and Surface Forces*, 2nd ed.; Academic Press: London, 1992.

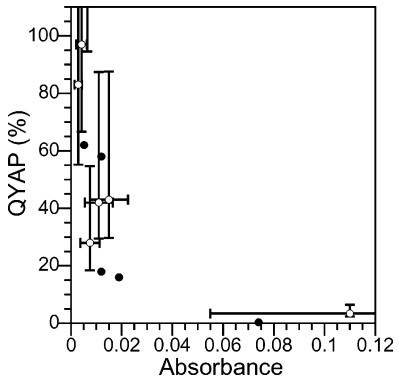

Figure 12. Quantum yield per absorbed photon (QYAP) of anodic photocurrent from SnS_2 electrodes sensitized by 1-6SQ as a function of peak absorbance measured in air. Dye deposition by the dipping method (○) and by the dropping method (●). Photocurrents were measured at an electrode potential of +0.7 V vs SCE. Aqueous electrolyte containing 10 mM hydroquinone as a regenerator was used.

system, namely Ru-based dyes on nanocrystalline TiO_2 films in which high quantum yields were obtained even at high dye coverages.

The sensitized photocurrent−voltage curve for 1-6SQ (Figure 10b) showed an onset potential closer to the E_{fb} of SnS_2 electrodes (∼0 V vs SCE) than the same curve measured for flat islands of 1-1OHSQ but reached a plateau at a similar potential (∼+0.6 V vs SCE). This behavior suggests that the regeneration reaction competes more effectively with the recombination reaction.[77] Possible mechanisms for the higher QYAP from 1-6SQ than from 1-1OHSQ will be discussed later. The photocurrents decreased after I−V measurements for the 1-6SQ systems especially when the irradiance was high. This apparent bleaching was more pronounced for the red side of the spectrum, and the photocurrent peak shifted to slightly shorter wavelengths. Dissolution of a population of less strongly bound dye aggregates from the surface into the electrolyte could occur if photooxidation of 1-6SQ is irreversible, since the positively charged oxidation product is expected to be more soluble in an aqueous solution than the neutral dye.

Figure 12 shows plots of QYAP values obtained for 1-6SQ layers at +0.7 V versus SCE against the peak optical absorbance. Error bars associated with the QYAP and absorbance values for the dipping experiments were estimated based on the ±50% potential error as was described previously for 1-1OHSQ. Note that the location of the point within the error limits depends on the actual absorbance value. QYAP values approaching 100% were observed for samples with a lower dye coverage, but QYAP values tended to quickly drop above 0.01 absorbance units a value that roughly corresponds to a tightly packed monolayer. Apparent quantum yields per absorbed photon greater than 100% were most likely due to unequal dye coverages on the two SnS_2 surfaces, where the more highly covered surface was selected for the photoelectrochemical experiments. If one considers exciton motion as diffusive, the diffusion length of an exciton should be larger than the thickness of the crystal in order to obtain a QYAP near unity. Assuming an absorbance of ∼0.01 corresponds to one monolayer, we find that Figure 12 implies that the diffusion length of an exciton perpendicular to the SnS_2 surface in 1-6SQ aggregates would be comparable to the molecular thickness (∼2−4 Å) if 1-6SQ formed perfectly packed layers. Our proposed mechanism for

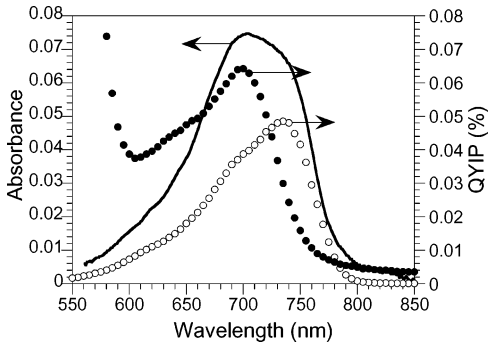

Figure 13. Vis−NIR absorption spectrum (solid curve) and photocurrent action spectra obtained at +0.7 V vs SCE (●, anodic photocurrent) and at 0.0 V vs SCE (○, cathodic photocurrent) for 8.7×10^{-10} mol cm^{-2} of 1-6SQ on SnS_2 prepared by the dropping method. Electrolyte containing 6.4 mM of $Ru(III)(NH_3)_6Cl_3$ was used.

the orientation of the dye chromophore is consistent with the short diffusion length of carriers in the thicker layers of 1-6SQ. Since the chromophores in the outside layers do not have face-to-face interactions with the chromophores of inside layers, charge transfer is not as facile perpendicular to the surface as it is along the J-aggregate direction parallel to the surface. Moreover, if impurities such as dichloromethane had been trapped between layers during aggregate formation, they could interfere with charge transport processes.

Peculiar Sensitization Behavior of 1-6SQ Multilayers. The thicker 1-6SQ dye layers showed a lower QYAP and less ideal sensitization behavior. These insulating organic layers require higher electric fields to drive the photogenerated carriers toward the interfaces. Also, a longer time was needed to establish an equilibrium throughout the dye layer. At a dye coverage of 2×10^{-10} mol cm^{-2} or more, an induction period of about 20 min was observed for photocurrent generation after application of a constant bias. Figure 11b shows spectra obtained for a dye coverage of $\sim 11 \times 10^{-10}$ mol cm^{-2} prepared by the dipping method. Application of low biases initially yielded cathodic photocurrents peaking at 700 nm (at 0.0 V vs SCE, open circles). Application of a more positive bias (+0.7 V vs SCE) resulted in the production of small anodic photocurrents that gradually increased to reach a stationary yield after nearly 3 h (closed circles).

Figure 11c compares photocurrent−voltage curves at different dye coverages under 690 nm illumination. As the dye concentration increases, the onset of anodic photocurrent, as well as the potential where the photocurrent saturates, shifts to more positive biases. For instance, curve d, obtained for the dye coverage of eleven monolayers, did not saturate until +1.0 V versus SCE. The recombination of electron−hole pairs created near the outer surface of the dye layer accounts for this behavior.

Cathodic photocurrent generation from 3D crystallites of 1-6SQ was studied using 6.4 mM $Ru(III)(NH_3)_6Cl_3$ as an electron acceptor for the photoelectrochemical measurements. Figure 13 shows absorption and photocurrent spectra obtained for a dye coverage of 8.7×10^{-10} mol cm^{-2} prepared by the dropping method (AFM image shown in Figure 8d). A cathodic photocurrent spectrum taken at 0.0 V versus SCE (open circles) had a peak at around 735 nm that is more efficient on the red side of the absorption band. Anodic photocurrents increased after the application of a positive bias, and the photocurrent spectrum at +0.7 V versus SCE (closed circles) showed a peak at around

700 nm, on the blue side of the absorption band. Obviously, a complex interplay between the interactions of the dye molecules with the surface and each other, charge transport within the dye layer, and charge transfer across the dye/semiconductor and dye/electrolyte interface are at work in this system.

Charge Injection/Recombination Mechanisms and Sensitization Yields for 1-1OHSQ and 1-6SQ. At a sufficiently positive bias, QYAP values near 100% were observed for ~0.3 to 1 monolayer coverages of 1-6SQ, whereas QYAP values only up to ~40% were observed for 1-1OHSQ layers with similar coverages. The excited singlet state lifetimes of 1-1OHSQ and its non-hydroxylated counterpart in dichloromethane solution were reported to be 3.0 and 1.5 ns, respectively,[80] and we would not expect a much shorter lifetime for 1-6SQ. The electron injection time observed for other monomeric organic dyes on the SnS_2 surface was significantly shorter (<10 ps for cresyl violet[81] and ~40 fs for oxazine[82]). When the favorable energy levels of the dye excited states depicted in Figure 3 are considered, electron injection yields of unity would be probable for both squaraine dyes. Under positive biases, injected electrons are driven into the bulk of SnS_2 by the electric field across the space charge layer. Tunneling of conduction band electrons back to the oxidized dye is unlikely considering the 0.1 μm width of the space charge layer at +0.7 V versus SCE for the moderately doped crystals used in this study. A simple consideration suggests that essentially all the injected electrons would escape the dye/semiconductor interface at biases where the photocurrents saturate. This seems to be realized for 1-6SQ but not for 1-1OHSQ. Two possibilities can be postulated to explain this observed behavior.

One possibility is that highly anisotropic electrical properties of SnS_2 enable the recombination path to persist despite increasing the strength of the electric field. Although SnS_2 single crystals used in this study are expected to have relatively few charge trapping sites, injected electrons could quickly find such a recombination channel due to the much higher mobility parallel to the surface.[83] If the dye oxidation potential is similar and the regeneration kinetics of hydroquinone is virtually the same, the comparison of photocurrent−voltage curves suggests that the recombination rate constant should be larger for 1-1OHSQ. Efficient recombination could be partly due to the proximity of the energy level of the oxidized dye to the conduction band of SnS_2, as shown in Figure 3. The flat-lying orientation of 1-1OHSQ could further facilitate orbital overlap with the recombination sites. On the other hand, a proposed edge-on orientation of 1-6SQ would reduce this overlap. The lack of red-shift in the absorption spectrum of adsorbed 1-6SQ at low coverages (Figures 10a and 11a) suggests a weaker electronic interaction of this dye with SnS_2 substrate. An interesting implication is that a strong electronic interaction with a semiconductor substrate may not necessarily be needed for an efficient charge injection. A similar effect may be at work in the nanocrystalline anatase solar cell. The metal-to-ligand charge transfer, occurring in the covalently bound Ru-bipyridine-based dye and subsequent electron injection into the TiO_2, is thought to inhibit the back reaction due to the distance of the oxidized Ru center from the electrode surface.[8]

A second possibility is related to the so-called special site model for fast electron injection. If only a portion of the adsorption sites allows fast injection of electrons, concentration quenching within the 1-1OHSQ monolayer could compete with the charge injection process. This mechanism was used to explain the slower fluorescence decays observed for cresyl violet adsorbed on SnS_2 upon increasing the dye coverage.[84] However, as shown previously, charge injection yields near unity are obtained for 1-6SQ on SnS_2 at similar dye coverages, so we feel that this mechanism is less likely unless very different injection or quenching mechanisms are involved for the two different systems. If indeed an effective intermolecular donor−acceptor coupling is realized by the proposed chromophore reorientation, a fast exciton delocalization within the 1-6SQ aggregate layer could possibly occur. This could enable excited electrons to find the "special site" more efficiently than flat-lying 1-10HSQ aggregates.

Conclusions

We have presented a study of the dye sensitization of semiconductor electrodes that combines optical absorption spectroscopy, photoelectrochemical measurements, and scanning probe measurements to understand the dye surface morphologies' influence on the sensitization process. Very efficient charge injection from excited dyes into the semiconductor conduction band was experimentally confirmed for a squaraine dye (1-6SQ) at surface concentrations up to one monolayer on *n*-doped SnS_2. Sensitization yield (QYAP) values approaching 100% were previously inferred for other dyes on WSe_2 and SnS_2 but without corresponding optical absorbance measurements.[9,10] Together with those studies, the present results support the idea that the layered dichalcogenide semiconductors have excellent properties for dye-sensitized photocurrent generation and can serve as model systems for understanding the sensitization process. Another squaraine dye (1-1OHSQ) exhibited slightly lower efficiency for photocurrent generation, yet maintained reasonably high QYAP values (10−40%) for both flat-lying monolayers and large 3D aggregates or microcrystallites. The probable cause for the observed difference in QYAP values between the two structurally similar squaraine dyes was interpreted as a result of different aggregate structures. The results also suggested that a competitive recombination pathway for photoinjected electrons with photooxidized dyes still exists on the nearly perfect van der Waals surfaces.

The present study infers that the further development of techniques for obtaining local information as well as bulk properties of individual and aggregated chromophores will be able to ultimately allow the understanding of the structure−property relationships for the dye sensitization processes. The next step may be an in situ combination of absorbance, photoelectrochemical measurements, and scanning probe microscopy to simultaneously investigate the morphology and spectral effects under operating conditions rather than in the sequential method presented herein. Further advances will allow

(80) Kamat, P. V.; Das, S.; Thomas, K. G.; George, M. V. *J. Phys. Chem.* **1992**, *96*, 195−199.
(81) Willig, F.; Eichberger, R.; Sundaresan, N. S.; Parkinson, B. A. *J. Am. Chem. Soc.* **1990**, *112*, 2702−2707.
(82) Lanzafame, J. M.; Miller, R. J. D.; Muenter, A. A.; Parkinson, B. A. *J. Phys. Chem.* **1992**, *96*, 2820−2826.
(83) Bucher, E. *Photoelectochemistry and Photovoltaics of Layered Semiconductors*; Aruchamy, A., Ed.; Kluwer Academic Publishers: Dordrecht, The Netherlands, 1992; pp 1−81.
(84) Eichberger, R.; Willig, F. *Chem. Phys.* **1990**, *141*, 159−173.

for photoelectrochemical investigation of individual dye molecules and aggregates.

Acknowledgment. We thank Professor Geoff Ashwell for supplying the 2,4-bis(4-(*N*-methyl-*N*-hexylamino)phenyl)squaraine (1-6SQ) and Greg Hagquist of Lexmark Corporation for providing the 2,4-bis(4-(*N*,*N*-dimethylamino)-2-hydroxyphenyl)-squaraine (1-1OHSQ) used in this study. We also thank Laura Sharp and Rick Laitenen for growing SnS_2 crystals and Michele Stawasz for helpful discussions. This work was supported by the Department of Energy Office of Basic Energy Sciences under Contract DE-F603-96ER14625.

Supporting Information Available: STM images showing the multiple layer adsorption of 1-6SQ on HOPG, an STM image of the ordered rows of 1-6SQ on HOPG, and a molecular model of the observed 1-6SQ row structure. This material is available free of charge via the Internet at http://pubs.acs.org.

JA0278483